Mon. Not. R. Astron. Soc. **309**, 100–112 (1999)

Giant radio sources

C. H. Ishwara-Chandra[1,2]★ and D. J. Saikia[1]★

[1]*National Center for Radio Astrophysics, TIFR, Post Bag 3, Ganeshkhind, Pune 411 007, India*
[2]*Joint Astronomy Programme, Department of Physics, Indian Institute of Science, Bangalore 560 012, India*

Accepted 1999 May 18. Received 1999 May 18; in original form 1998 November 23

ABSTRACT

We present multifrequency Very Large Array (VLA) observations of two giant quasars, 0437−244 and 1025−229, from the Molonglo Complete Sample. These sources have well-defined FR II radio structure, possible one-sided jets, no significant depolarization between 1365 and 4935 MHz and low rotation measure ($|\mathrm{RM}| < 20\,\mathrm{rad\,m^{-2}}$). The giant sources are defined to be those with overall projected size $\geqslant$1 Mpc. We have compiled a sample of about 50 known giant radio sources from the literature, and have compared some of their properties with a complete sample of 3CR radio sources of smaller sizes to investigate the evolution of giant sources, and test their consistency with the unified scheme for radio galaxies and quasars. We find an inverse correlation between the degree of core prominence and total radio luminosity, and show that the giant radio sources have similar core strengths to smaller sources of similar total luminosity. Hence their large sizes are unlikely to be caused by stronger nuclear activity. The degree of collinearity of the giant sources is also similar to that of the sample of smaller sources. The luminosity–size diagram shows that the giant sources are less luminous than our sample of smaller sized 3CR sources, consistent with evolutionary scenarios in which the giants have evolved from the smaller sources, losing energy as they expand to these large dimensions. For the smaller sources, radiative losses resulting from synchrotron radiation are more significant while for the giant sources the equipartition magnetic fields are smaller and inverse Compton loss owing to microwave background radiation is the dominant process. The radio properties of the giant radio galaxies and quasars are consistent with the unified scheme.

Key words: polarization – galaxies: active – galaxies: jets – galaxies: nuclei – quasars: general – radio continuum: galaxies.

1 INTRODUCTION

Giant radio sources (GRSs), defined to be those with a projected linear size $\geqslant$1 Mpc ($q_0 = 0.5$ and $H_0 = 50\,\mathrm{km\,s^{-1}\,Mpc^{-1}}$), are the largest single objects in the Universe, and are extremely useful for studying a number of astrophysical problems. These range from understanding the evolution of radio sources and constraining orientation-dependent unified schemes to probing the intergalactic medium at different redshifts (e.g. Saripalli 1988; Subrahmanyan & Saripalli 1993; Subrahmanyan, Saripalli & Hunstead 1996; Mack et al. 1998; Schoenmakers et al. 1998). There are about 50 known giant sources, only five of which are quasars, the largest being the radio galaxy 3C236 with a projected linear size of 5.7 Mpc (Willis, Strom & Wilson 1974; Strom & Willis 1980; Barthel et al. 1985). In the complete sample of 3CR radio sources (Laing, Riley & Longair 1983), about 6 per cent of the radio sources are giants. The GRSs are usually of low radio luminosity, with values often in the transition region between the FR I and FR II type sources (Fanaroff & Riley 1974), and are believed to be advancing outwards through the low-density (10^{-5}–$10^{-6}\,\mathrm{cm^{-3}}$) intergalactic medium. Their spectral ages have been estimated to be about 10^7 to 10^8 yr (e.g. Mack et al. 1998), but these values are dependent on a number of assumptions and have to be treated with caution (e.g. Eilek, Melrose & Walker 1997).

In this paper we report further observations of two giant quasars (GQs), 0437−244 and 1025−229, which we had earlier observed as part of our study of the depolarization properties of a well-defined sample of radio sources selected from the Molonglo Complete Sample (Ishwara-Chandra et al. 1998, hereinafter referred to as IC98, and references therein). The quasar 0437−244 at a redshift of 0.84 is at present the highest redshift giant quasar known. The paper is organized as follows. In Section 2, observations of the two giant quasars from the Molonglo Sample are presented. In Section 3, we list some of the properties of known giant radio galaxies and quasars, and discuss their consistency with proposed evolutionary scenarios for these

★ E-mail: ishwar@ncra.tifr.res.in (CHIC); djs@ncra.tifr.res.in (DJS)

objects. In Section 4, we examine the consistency of the giant sources with the unified schemes for radio sources, and possible effects of the environment. The conclusions are summarized in Section 5.

2 GIANT QUASARS FROM THE MOLONGLO SAMPLE

In this section we present the observations and observational results of the two giant quasars 0437−244 and 1025−229 from the Molonglo complete sample. The GQ 0437−244 has an angular size of 128 arcsec, which corresponds to a projected linear size of 1.06 Mpc at a redshift of 0.84. This is presently the highest redshift GQ; the only other known GQ with a redshift greater than 0.5 is 1127−300 (Bhatnagar, Gopal-Krishna & Wisotzki 1998) which is at a redshift of 0.6337. The second GQ, 1025−229, is relatively nearby at a redshift of 0.309, and has an angular size of 198 arcsec, which corresponds to a linear size of 1.11 Mpc. The luminosities at 1.4 GHz are 2.88×10^{27} and 3.47×10^{26} W Hz^{-1} for 0437−244 and 1025−229 respectively.

Table 1. Observing log.

Array conf.	Obs. band	Obs. freq. (MHz)	Bandwidth (MHz)	Date of obs.
BnA	L	1365	50	1995 Sep 20
	L	1665	25	
CnB	C	4635	50	1996 Jan 20,31
	C	4935	50	
DnC	U	14965	50	1997 Oct 3, 12
BnA	X	8447	25	1997 Feb 3

2.1 Observations and analyses

The sources were observed in the *L*, *C*, *X* and *U* bands with the Very Large Array (VLA), and the observing log is summarized in Table 1. The observations in the *L*, *C* and *U* bands were scaled-array ones, while those in the *X*-band were made with a higher resolution. The *L*- and *C*-band total-intensity and linear-polarization images have been reported earlier by IC98. However, the spectral index and rotation measure estimates based on these images are presented here. All the data were calibrated in the standard way using the NRAO AIPS package. The final images in the *L*, *C* and *U* bands were restored with a beam of 4.5×3.2 arcsec^2 along PA $= -70°$ for 0437−244, and 8.0×4.5 arcsec^2 along PA $= -50°$ for 1025−229. The restoring beam for the BnA-array observations at the *X* band is 1.89×0.58 arcsec^2 along PA $= 35°$ for 0437−244, and 0.80×0.61 arcsec^2 along PA $= 53°$ for 1025−229. The images in the *X* and *U* bands have been corrected for primary beam attenuation. The *U*-band images have not been self-calibrated because they have low signal-to-noise ratio. Some of the observed parameters are presented in Table 2.

2.2 Observational results

2.2.1 0437−244

In Fig. 1(a) we present the total-intensity image at 1365 MHz with the spectral index between 1365 and 4935 MHz superimposed in grey. The scaled-array 15-GHz image and the high-resolution 8.4-GHz image are presented in Figs 1(b) and (c) respectively.

The GQ 0437−244 is a classical double-lobed FR II radio source with well-defined hotspots at the outer edges, a core contributing about 10 per cent of the total flux density at an

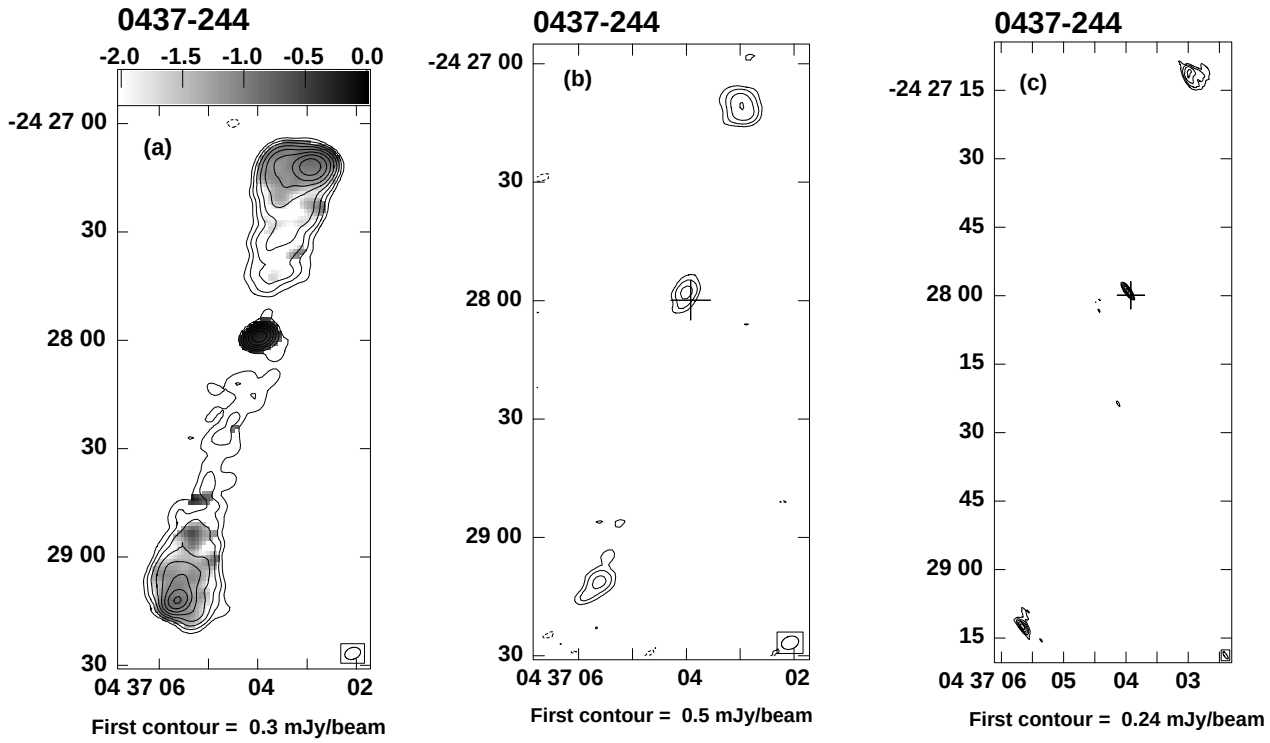

Figure 1. Radio images of 0437 − 244. (a) Total-intensity image at 1365 MHz with an angular resolution of 4.5×3.2 arcsec^2 along PA $= -70°$; the spectral index between 1365 and 4935 MHz is superimposed in grey. (b) The 15-GHz image with the same resolution as in (a). (c) The high-resolution image at 8.4 GHz with an angular resolution of 1.89×0.58 arcsec^2 along PA $= 35°$. Contour levels are at -2, -1, 1, 2, 4, 8, 16, … times the first contour that is shown below each image. The cross marks the position of the optical quasar.

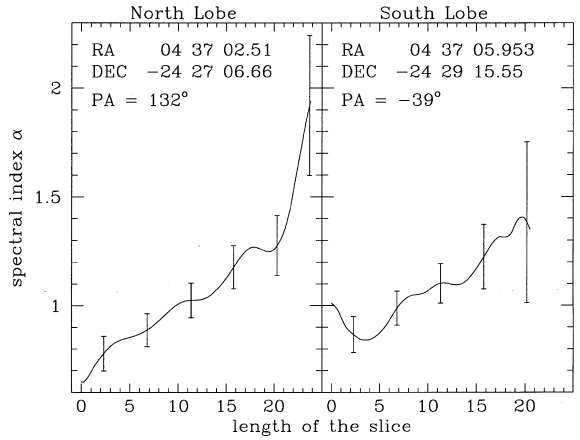

Figure 2. The variation in spectral index between 1365 and 4935 MHz for the northern and southern lobes of 0437 − 244 along the position angles of the slices indicated in the panels above. The positions of the origins in the lobes are also listed above. The error bars indicate $\pm 1\sigma$ errors for the spectral indices.

emitted frequency of 8 GHz, and signs of a possible jet towards the southern component. The spectral indices, α (defined as $S \propto \nu^{-\alpha}$), at the peaks of emission in the outer lobes are about 0.6 and 0.9 for the northern and southern components respectively. In both components the spectral indices steepen significantly up to distances of about 20 arcsec (about 170 kpc) from the peaks of emission (Fig. 2). The errors in the spectral indices have been estimated assuming an error of 3 per cent in the measured flux density. Adopting the formalism of Myers & Spangler (1985), the age estimates as a result of synchrotron radiative losses in the Kardashev–Pacholczyk model (Pacholczyk 1977) are 5.8×10^7 and 2.7×10^7 yr for the northern and southern lobes respectively. The injection spectra have been estimated from the spectral indices of the hotspots, which have been defined to be the peaks of emission in the outer lobes. The integrated spectra of the northern and southern lobes are straight between 1.4 and 15 GHz, with spectral indices of 1.16 ± 0.07 and 1.10 ± 0.09 respectively, because these are dominated by the hotspots. The core has a flat spectrum between 1.4 and 8.4 GHz, with a spectral index of 0.23 ± 0.10, but shows evidence of steepening between 8.4 and 15 GHz, with a spectral index of 1.50 ± 0.24. Such a steep spectral index is uncommon; this is the only quasar in our sample of Molonglo radio sources (cf. IC98) with a core spectral index between 8.4 and 15 GHz that is steeper than about 0.5. The steep core spectrum is possibly caused by variability of the core flux density. The integrated spectrum of the entire source between 408 MHz and 15 GHz is 0.94 ± 0.05.

We have computed the rotation measures for both lobes of the giant quasars using two widely spaced *L*-band (1365 MHz and 1665 MHz) frequencies and the *C*-band (4935 MHz) frequencies. For 0437−244, the northern lobe has an integrated rotation measure (RM) of about 13.6 ± 1.3 rad m^{-2}, while for the southern lobe the RM is about 4.2 ± 3.4 rad m^{-2}. The depolarization parameter, defined to be the ratio of the degree of polarization at 1365 MHz to that at 4935 MHz, is close to about 1, indicating that there is no significant depolarization until about 1365 MHz (cf. IC98).

2.2.2 1025−229

This is also a well-defined FR II radio source with two hotspots in the southern lobe, a core contributing about 12 per cent of the total flux density of the source, and a jet-like structure close to the radio core (Figs 3a–d). The high-resolution 8.4-GHz image of the core region resolves the core and the jet-like structure; the latter consists of two components along a PA of −7°. This is significantly different from the PA of −38° defined by the core and the northern hotspot (Figs 3c and d). A deep optical image might help clarify whether this feature is an unrelated source. However, the similarity in RM of the jet-like feature and the lobes, which are listed later in this section, suggests that these might be related. The spectral index slices for the two lobes are presented in Fig. 4. The spectral index of the northern hotspot is about 0.9 and steepens to about 1.5 over a distance of 40 arcsec (about 220 kpc), while for the southern lobe both the peaks of emission have a spectral index of 0.6 which steepens to about 1.7 over a distance of about 40 arcsec. Adopting the formalism of Myers & Spangler (1985), the age estimates as a result of synchrotron radiative losses in the Kardashev–Pacholczyk model (Pacholczyk 1977) are 7.8×10^7 and 1.2×10^8 yr for the northern and southern lobes respectively. The injection spectra have again been estimated from the hotspot spectral indices. Estimating the ages for a subset of 10 sources chosen at random from our Molonglo sample (IC98) yields ages in the range $0.6–6.5 \times 10^7$ yr with a median value of about 2.3×10^7 yr. The integrated spectral indices of the northern and southern lobes between 1365 MHz and 15 GHz are 1.31 ± 0.09 and 1.08 ± 0.06, respectively. The spectral index of the entire source is 0.90 ± 0.04 between 408 MHz and 15 GHz, while that of the core is 0.26 ± 0.10 between 1.665 and 15 GHz. The depolarization parameter between 1365 and 4935 MHz is again close to about 1, while the rotation measures estimated from the two *L*-band frequencies (1365 and 1665 MHz) and *C*-band data are -21.3 ± 2.3, -15.3 ± 0.9 and -21.5 ± 3.6 rad m^{-2} for the northern and southern lobes and the steep-spectrum jet-like feature close to the radio core.

3 THE SAMPLE OF GIANT RADIO SOURCES

To understand the evolution of GRSs, examine their consistency with the unified schemes and use them as probes of their environment and the intergalactic medium, we have compiled a sample of known giant radio sources from the literature. A GRS is defined to be one with an overall projected linear size $\geqslant 1$ Mpc. Our sample of known GRSs consists of 53 sources, 48 of which are associated with galaxies and the remaining five with quasars. These are listed in Table 3, which is arranged as follows. Columns 1 and 2: source name and an alternative name. Most sources have peaks of emission in the outer parts of the lobes and either belong to FR II or are in the FR I/FR II transition region. Those with a clear FR I structure, such as 3C129 and 3C130, are marked with an asterisk in column 1. Column 3: optical identification, where 'G' and 'Q' denote galaxy and quasar respectively; column 4: redshift; columns 5 and 6: the largest angular size in arcsec and the corresponding projected linear size in Mpc; column 7: the luminosity at 1.4 GHz in units of W Hz^{-1}; column 8: the fraction of emission from the core, f_c, at an emitted frequency of 8 GHz, with a ' $\sim$ ' sign indicating those sources for which the core flux density has been estimated by us from the available images; columns 9 and 10: the minimum energy density, $u_{\rm min}$, in units of 10^{-14} J m^{-3}, and the equipartition magnetic field, $B_{\rm eq}$, in nT ($1\,{\rm T} = 10^4$ G); column 11: the ratio, r_θ, defined to be > 1, of the separation of the oppositely directed components from the

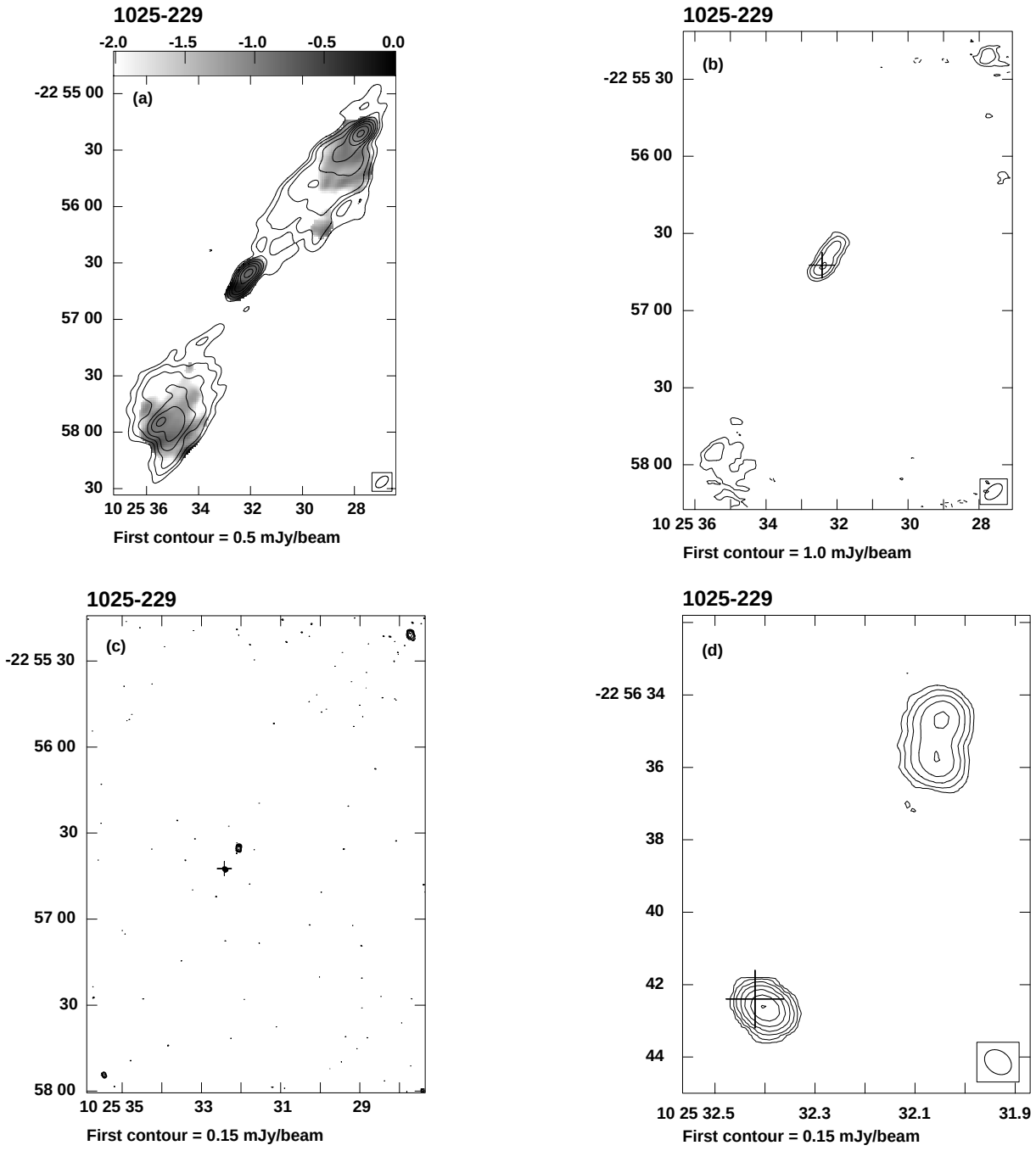

Figure 3. Radio images of 1025 − 229. (a) Total-intensity image at 1365 MHz with an angular resolution of 8.0×4.5 arcsec^2 along PA $= -50°$; the spectral index between 1365 and 4935 MHz is superimposed in grey. (b) The 15-GHz image with the same angular resolution as in (a). (c) The high-resolution image at 8.4 GHz of the entire source with an angular resolution of 0.80×0.61 arcsec^2 along PA $= 53°$. (d) The high-resolution 8.4-GHz image of the core and the component close to it. Contour levels are at -2, -1, 1, 2, 4, 8, 16, … times the first contour that is shown below each image. The cross marks the position of the optical quasar.

nucleus; column 12: the misalignment angle, Δ, defined to be the supplement of the angle formed at the nucleus by the outer hotspots; column 13: references for the radio structure. The minimum energy density and equipartition magnetic field have been estimated (Miley 1980; Longair 1994) for the extended emission assuming a cylindrical geometry, a filling factor of unity and that energy is distributed equally between relativistic electrons and protons. The size of the lobes has been estimated from the lowest contours in the available images, and the core flux density has been subtracted while estimating the minimum energy density. In the case of a few sources, such as the 7C ones, for which reliable lobe sizes could not be obtained, $u_{\rm min}$ and $B_{\rm eq}$ have not been listed in the table. The luminosity has been estimated between 10 MHz and 10 GHz using the known spectral indices of the extended emission. For estimating the error in $u_{\rm min}$ we have assumed errors of 5 per cent in the flux density, 0.1 in spectral index and 25 per cent in the volume.

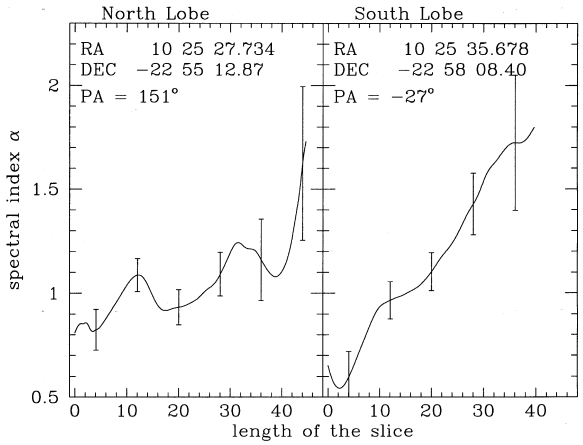

Figure 4. The variation in spectral index between 1365 and 4935 MHz for the northern and southern lobes of 1025 − 229 along the position angles of the slices indicated in the panels above. The positions of the origins in the lobes are also listed above. The error bars indicate $\pm 1\sigma$ errors for the spectral indices.

3.1 Energy density and magnetic field

The minimum energy density is in the range 0.4 to 162×10^{-14} J m^{-3} with a median value of about 4.4×10^{-14} J m^{-3}, while the equipartition magnetic field for the lobes range from 0.06 to 1.25 nT with a median value of 0.2 nT. The minimum energy density might be expected to increase with redshift, because of better confinement by the intergalactic medium and greater dissipation of energy by the beams interacting with a denser environment. An earlier study by Subrahmanyan & Saripalli (1993) showed marginal evidence of an increase in minimum energy density or pressure with redshift. However, it is important to confirm whether such trends might be caused by possible selection effects. For example, if the giant sources are chosen from a given flux-density-limited sample, luminosity and minimum energy density could be strongly correlated with redshift, because most sources are close to the flux density limit of the survey. Although the giant radio sources in our sample have been selected from surveys ranging from the 3CR to the Westerbork Northern Sky Survey (WENSS) (Laing et al. 1983; Rengelink et al. 1997), the observed range in flux density at, say, 1.4 GHz for almost all the objects for which we have been able to evaluate $u_{\rm min}$ is within one order of magnitude, while the luminosity spans about three orders of magnitude. Thus although the luminosity and minimum energy density appear correlated with redshift (Figs 5a and b), with Spearman rank correlation coefficients of 0.90 and 0.68 respectively, we need to identify a large number of giant sources from surveys such as WENSS and the NRAO Sky Survey (NVSS) to determine whether there is a genuine trend for the minimum energy density to increase with redshift.

3.2 Evolution of giant radio sources

We investigate the evolution of the giant radio sources by plotting them in a power–linear size or P–D diagram along with the complete sample of 3CR (Laing et al. 1983) radio sources. The P–D diagram is, in principle, a powerful tool for investigating the temporal evolution of radio sources (Shklovskii 1963; Scheuer 1974), although in practice the detailed interpretation is debatable (cf. Baldwin 1982; Kaiser et al. 1997; Blundell, Rawlings & Willott 1999). One must also be careful of possible selection effects, because large sources with weak lobes or cocoons may sometimes appear to be disconnected and hence misclassified as independent sources. Also, weak FR I sources with diffuse extended lobes may have only the bright inner parts detected at large redshifts and hence appear smaller in size (cf. Neeser et al. 1995). However, all but four of the GRSs are clear FR IIs or are in the FR I/II transition region and have well-defined peaks of emission towards their outer edges. Hence their parameters are unlikely to be affected by such selection effects. The P–D diagram for the complete sample of 3CR radio sources with sizes between 50 kpc and 1 Mpc, and all the giant sources (Fig. 6) show that there is a clear deficit of giant sources (> 1 Mpc) with high radio luminosity, suggesting that the luminosity of radio sources

Table 2. Observed parameters of the giant quasars.

Source name	Freq	rms noise	Comp.	Peak	Int.	*m*
0437−244	1365	100	N Lobe	66.2	281.2	8.0
			S Lobe	44.1	165.6	12.2
			Core	16.9	18.2	< 0.8
			Total		471	
	1665	150	N Lobe	53.4	198.8	7.7
			S Lobe	35.8	106.7	9.2
			Core	15.2	16.0	< 1.1
			Total		321	
	4635	55	N Lobe	22.2	74.5	8.2
			S Lobe	15.9	42.5	10.3
			Core	12.9	13.6	< 0.9
			Total		130	
	4935	55	N Lobe	20.3	66.6	7.8
			S Lobe	14.8	38.7	6.7
			Core	12.5	13.0	< 0.9
			Total		121	
	8450	45	N Lobe	2.2	19.2	–
			S Lobe	5.7	17.0	–
			Core	10.5	11.6	–
			Total		46.6	
	14965	170	N Lobe	4.2	15.1	–
			S Lobe	2.8	6.63	–
			Core	2.7	4.91	–
			Total		30.9	
1025−229	1365	165	N Lobe	78.6	286.5	9.0
			S Lobe	18.4	211.1	10.7
			Core	13.5	21.8	< 0.7
			Total		560	
	1665	150	N Lobe	64.3	214.5	8.8
			S Lobe	16.6	155.1	10.5
			Core	11.0	16.91	< 1.0
			Total		421	
	4635	65	N Lobe	28.2	66.9	7.1
			S Lobe	6.5	39.2	10.2
			Core	10.1	11.2	< 1.0
			Total		128	
	4935	70	N Lobe	26.1	59.8	8.5
			S Lobe	6.0	39.2	8.5
			Core	10.2	11.2	< 1.0
			Total		118	
	8450	45	N Lobe	3.2	15.9	–
			S Lobe	0.8	1.95	–
			Core	10.0	11.03	–
			Total		40	
	14965	230	N Lobe	3.8	8.23	–
			S Lobe	3.8	17.8	–
			Core	8.7	10.0	–
			Total		36	

Notes. Frequency is expressed in MHz, rms in units of μJy beam^{-1}, peak flux densities in units of mJy beam^{-1} and integrated flux density in mJy; *m* is the scalar percentage polarization.

Table 3. The sample of giant radio sources.

Source name	Other name	ID	z	LAS (arcsec)	LLS (Mpc)	$P_{1.4}$ ($W\,Hz^{-1}$)	f_c	u_{min} ($J\,m^{-3}$)	B_{eq} (nT)	r_θ	Δ (°)	Ref.
0017−205	MRC	G	0.197	372	1.55	26.20	0.063	–	–	1.41	3	1
0055+300	NGC 315	G	0.0167	3480	1.64	24.82	0.32	1.94	0.137	2.04	9	2,3
0109+492	3C35	G	0.067	635	1.10	25.64	0.035	2.46	0.154	1.06	5	4
0114−476	PKS	G	0.146	702	2.35	26.51	∼0.012	4.25	0.202	1.39	18	5
0132+376	3C46	G	0.4373	163	1.09	27.21	0.0078	38.74	0.611	1.56	7	6
0136+397	4C39.04	G	0.2107	343	1.50	26.30	0.016	4.49	0.208	1.19	2	7,8
0157+405	4C40.08	G	0.078	840	1.67	25.62	0.018	0.99	0.098	2.54	0	8,9
0211−479	PKS	G	0.2195	378	1.70	26.54	∼0.0069	6.68	0.254	1.15	1	5
0309+411	B3	G	0.136	570	1.80	26.01	0.54	0.97	0.097	1.67	14	10
0313+683	WENSS	G	0.0902	894	2.01	25.64	0.19	4.46	0.207	1.45	6	11
0313−271	MRC	G	0.216	227	1.01	26.06	0.011	3.31	0.179	1.25	10	1
0319−454	PKS	G	0.0633	1538	2.54	25.81	0.023	1.57	0.123	2.22	1	12
0424−728	PKS	G	0.1921	346	1.42	26.51	∼0.039	12.41	0.346	1.09	6	5
0437−244	MRC	Q	0.84	128	1.06	27.46	0.10	47.50	0.677	1.54	0	13
0445+449*	3C129	G	0.021	1800	1.06	25.21	0.023	6.53	0.251	–	–	4
0448+519*	3C130	G	0.109	584	1.54	26.29	0.043	5.22	0.224	–	–	4
0503−286	MRC	G	0.038	2400	2.48	25.26	∼0.029	1.28	0.111	1.89	14	14,15
0511−305	PMN	G	0.0583	684	1.05	25.70	0.017	3.93	0.195	1.88	18	5
0634−205	PMN	G	0.056	810	1.20	26.07	<0.021	7.17	0.263	1.32	2	16,17
0654+482	7C	G	0.776	135	1.10	26.69	–	–	–	–	–	18
0707−359	PKS	G	0.2182	492	2.21	26.71	∼0.10	8.03	0.278	1.44	7	5
0744+558	DA240	G	0.0356	2040	1.99	25.50	0.077	0.61	0.077	1.39	2	19,20
0821+695	8C	G	0.538	402	2.94	26.29	0.22	3.23	0.177	1.12	1	21
0915+320*	B2	G	0.062	660	1.07	24.69	0.14	2.12	0.143	–	–	22
0945+734	4C73.08	G	0.0581	884	1.35	25.77	0.024	1.68	0.127	1.70	6	4
1003+351	3C236	G	0.0988	2340	5.70	26.41	0.46	1.32	0.113	1.68	2	19,23,24
1025−229	MRC	Q	0.309	198	1.11	26.54	0.12	16.73	0.402	1.25	8	13
1029+571*	HB13	G	0.034	1110	1.03	24.50	0.19	4.30	0.204	–	–	25
1058+368	7C	G	0.75	158	1.22	26.86	–	–	–	–	–	18
1127−130	PKS	Q	0.6337	297	2.30	27.53	0.087	6.93	0.259	1.21	0	26
1144+352	WENSS	G	0.063	701	1.15	25.09	0.95	1.18	0.107	1.20	10	27
1158+351	87GB	G	0.55	140	1.03	26.79	0.015	33.22	0.566	1.24	5	28
1209+745	4C74.17	G	0.107	420	1.09	25.52	0.089	2.59	0.158	1.55	18	29
1218+639	TXS	G	0.2	420	1.77	26.69	–	–	–	–	–	30
1232+216	3C274.1	G	0.422	152	1.00	27.32	0.031	47.53	0.677	1.21	6	31
1312+698	DA340	G	0.106	420	1.09	25.93	–	–	–	–	–	30
1331−099	PKS	G	0.081	820	1.68	26.06	0.11	4.84	0.216	1.09	3	32
1349+647	3C292	G	0.71	133	1.06	28.09	0.0013	162.53	1.252	1.12	3	31
1358+305	B2	G	0.206	649	2.80	26.03	0.011	1.17	0.106	2.13	5	33
1452−517	MRC	G	0.08	1218	2.48	25.66	0.35	1.10	0.103	1.60	12	8,34
1519+513	87GB	G	0.37	258	1.59	27.06	0.017	18.20	0.419	1.08	0	28
1545−321	PKS	G	0.1085	498	1.31	26.03	<0.032	12.29	0.344	1.02	4	5
1549+202	3C326	G	0.0895	1173	2.63	26.15	0.012	2.00	0.139	1.95	3	35
1602+376	7C	G	0.814	175	1.44	26.93	–	–	–	–	–	18
1626+518	WENSS	G	0.056	1140	1.68	25.10	0.14	–	–	1.44	5	36
1636+418	7C	G	0.867	130	1.09	26.67	–	–	–	–	–	18
1637+826	NGC 6251	G	0.023	3120	2.00	24.66	0.75	0.38	0.061	1.71	26	37,38
1701+423	7C	G	0.476	180	1.24	26.47	–	–	–	–	–	18
1721+343	4C34.47	Q	0.2055	244	1.05	26.51	0.60	8.02	0.278	1.05	1	39,40
1834+620	WENSS	G	0.519	197	1.42	27.19	–	20.85	0.449	1.03	0	41
1910−800	PKS	G	0.346	366	2.18	26.79	∼0.059	10.16	0.313	1.06	0	5
2043+749	4C74.26	Q	0.104	610	1.55	26.03	0.51	3.02	0.171	1.04	7	42
2309+184	3C457	G	0.427	205	1.36	27.38	0.013	32.96	0.564	1.00	6	43

References: 1. Kapahi et al. (1998b); 2. Bridle et al. (1976); 3. Willis et al. (1981); 4. Jägers (1986); 5. Subrahmanyan, Saripalli & Hunstead (1996); 6. Gregorini et al. (1988); 7. Hine (1979); 8. Saripalli (1988); 9. Vigotti et al. (1989); 10. de Bruyn (1989); 11. Schoenmakers et al. (1998); 12. Saripalli, Subrahmanyan & Hunstead (1994); 13. Present work; 14. Saripalli et al. (1986); 15. Subrahmanya & Hunstead (1986); 16. Danziger, Goss & Frater (1978); 17. Kronberg, Wielebinski & Graham (1986); 18. Cotter, Rawlings & Saunders (1996); 19. Willis, Strom & Wilson (1974); 20. Strom, Baker & Willis (1981); 21. Lacy et al. (1993); 22. Ekers et al. (1981); 23. Strom & Willis (1980); 24. Barthel et al. (1985); 25. Masson (1979); 26. Bhatnagar, Gopal-Krishna & Wisotzki (1998); 27. Schoenmakers et al. (1999); 28. Machalski & Condon, (1985); 29. van Breugel & Willis (1981); 30. Saunders, Baldwin & Warner (1987); 31. Alexander & Leahy (1987); 32. Saripalli et al. (1996); 33. Parma et al (1996); 34. Jones & McAdam (1992); 35. Willis & Strom (1978); 36. Röttgering et al. (1996); 37. Waggett, Warner & Baldwin (1977); 38. Willis et al. (1982); 39. Jägers et al. (1982); 40. Barthel (1987); 41. de Bruyn et al. (1998); 42. Riley et al (1989); 43. Leahy & Perley (1991).

decreases as they evolve. This trend was suggested earlier (Baldwin 1982; Cotter, Rawlings & Saunders 1996; Kaiser & Alexander 1997; Kaiser et al. 1997) using small samples of giant sources, and has now been established with a sample of over 50 giant radio sources. Our sample of 53 giant sources includes all those from a complete sample of sources selected from the Molonglo Reference Catalogue (MRC) (Large et al. 1981; Kapahi et al. 1998a,b and references therein), and early results from the

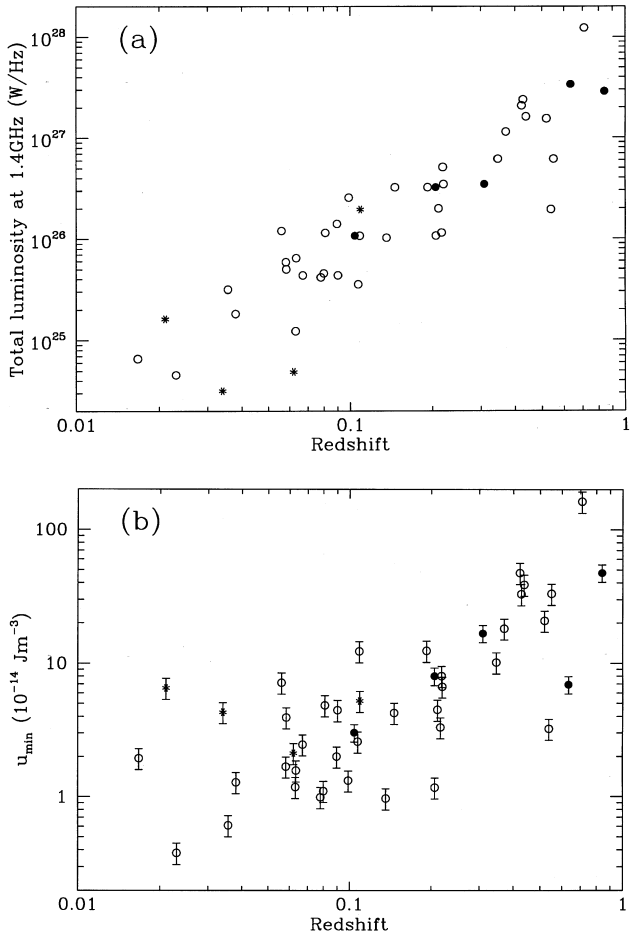

Figure 5. (a) The total radio luminosity at 1.4 GHz and (b) the minimum energy density of the lobes against the redshift of the giant radio sources. Filled circles denote quasars, while open circles denote all radio galaxies except those with a clear FR I structure, which have been marked with an asterisk.

WENSS survey, in addition to the searches for giants undertaken by Cotter et al. (1996) from the 7C survey and Subrahmanyan et al. (1996) from the MRC. Given the range of surveys and the systematic searches for giant sources, the dearth of giant objects with high radio luminosity is unlikely to be caused by any selection effects. There is also a sharp cut-off in the sizes of the GRSs at about 3 Mpc, with only one exception, namely 3C236, which has a size of 5.7 Mpc. To investigate whether there are larger sources that may have been missed, one requires low-frequency surveys with higher sensitivity to diffuse, low-brightness emission. In Fig. 6, we superimpose the evolutionary tracks suggested by Kaiser et al. (1997) for three different jet powers and find that our sample of giant sources is roughly consistent with their self-similar models where the lobes lose energy because of expansion and radiative losses caused by both inverse-Compton and synchrotron processes. In the models developed by Blundell et al. (1999), the luminosity declines more rapidly than the Kaiser et al. tracks, and provides a somewhat better fit to the upper envelope for large linear sizes. The P–D diagram, along with these evolutionary models, suggests that the progenitors of the giants are normal FR II or FR I radio sources, depending on their jet power, and the giant sources do not represent objects with unusually large nuclear engines or increased activity in the nucleus.

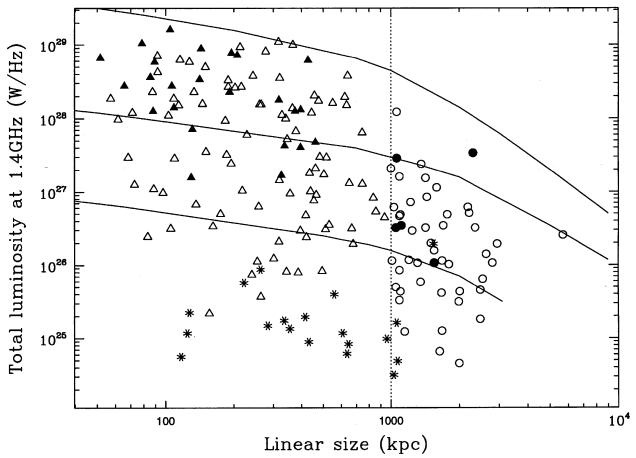

Figure 6. The luminosity–linear size or P–D diagram for all 3CR sources with 50 kpc $< D <$ 1 Mpc and our sample of giant sources. The giant quasars and galaxies are shown by filled and open circles respectively, while the 3CR quasars and galaxies are shown by filled and open triangles respectively, except for those with a clear FR I structure. The FR I sources are marked with an asterisk. The evolutionary scenarios for sources with jet powers of 1.3×10^{40}, 1.3×10^{39} and 1.3×10^{38} W from Kaiser, Dennett-Thorpe & Alexander (1997) are shown superimposed on the diagram.

3.3 Radiation losses in giant sources

In this section we investigate the relative importance of synchrotron and inverse-Compton losses in the evolution of giant radio sources. The equipartition magnetic fields of the lobes for almost all the giant sources are less than the equivalent magnetic field of the microwave background radiation, suggesting that inverse-Compton losses are larger than synchrotron radiative losses in the evolution of the lobes of these giant sources. For comparison, we have computed the equipartition magnetic field for all the sources, except 3C293 and 3C321, which are in the 3CR complete sample and have been observed by Leahy & Williams (1984), Leahy, Muxlow & Stephens (1989), Leahy & Perley (1991), Fernini et al. (1993), Johnson, Leahy & Garrington (1995), Fernini, Burns & Perley (1997) and Hardcastle et al. (1997), and also the corresponding inverse Compton field, $B_{ic} = 0.32(1+z)^2$ nT, at the redshift of the source. The above two sources were excluded because their bridges have not been well-mapped. A plot of the linear size of the radio source against the ratio of inverse Compton field to equipartition magnetic field (Fig. 7a) shows that synchrotron losses dominate over inverse Compton losses for almost all objects below about a Mpc while the reverse is true for the giant sources. This is also illustrated in Fig. 7(b), where we plot the linear size against the ratio $B_{eq}^2/(B_{ic}^2 + B_{eq}^2)$, which represents the ratio of the energy loss by synchrotron radiation to total energy loss resulting from both the processes. The ratio is close to 1 for the small sources, lies between about 0.5 and 1 for sources smaller than a Mpc, and falls sharply for the giant sources to a value of about 0.05. This is consistent with similar suggestions made earlier by Gopal-Krishna, Wiita & Saripalli (1989). As the sample of giant radio sources has been compiled from a large number of surveys complete to different flux density limits, we have checked and confirmed these trends by considering 3CR and giant sources over a similar luminosity range of 10^{25} to 10^{27} W Hz^{-1}. This range was chosen to maximize the number of 3CR and giant radio sources in a similar luminosity

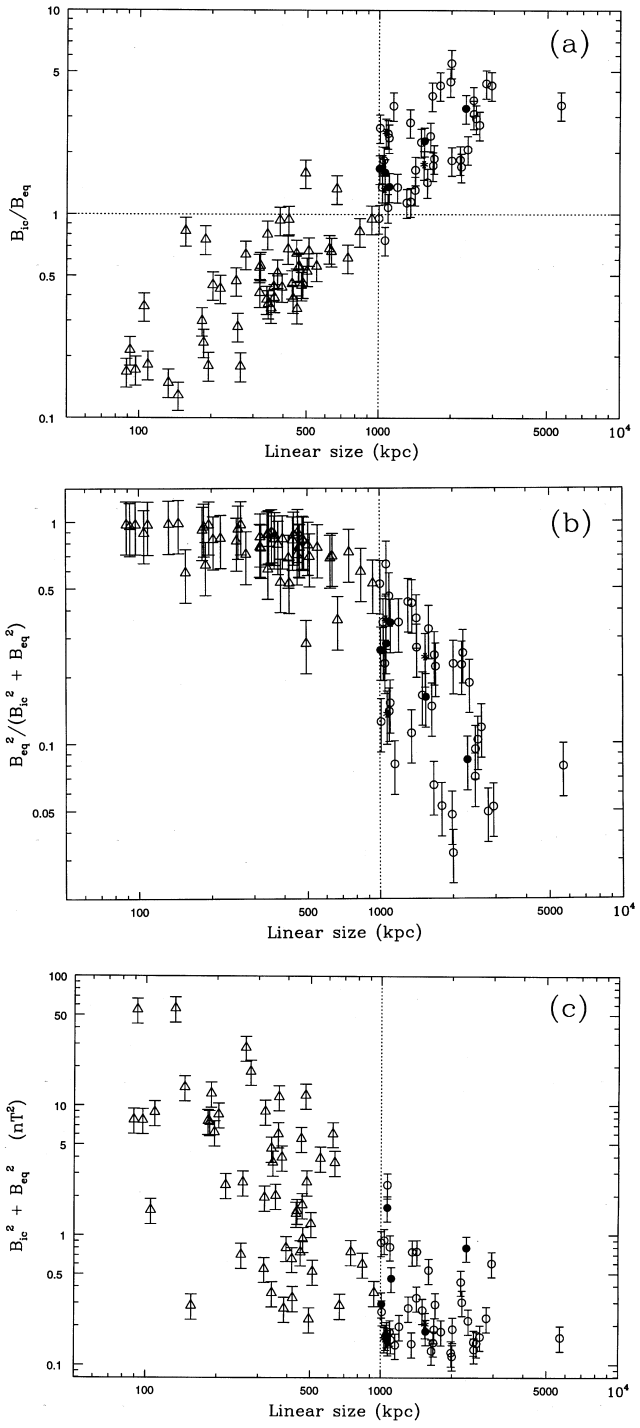

Figure 7. (a) The ratio B_{ic}/B_{eq}, (b) the ratio $B_{eq}^2/(B_{ic}^2 + B_{eq}^2)$ and (c) $B_{ic}^2 + B_{eq}^2$ plotted against the projected linear size of the sample of giant and smaller sources. In panel (c), the scale of the *y*-axis is in units of nT^2, while the *x*-axis is in kpc in all the above panels. The giant quasars and galaxies are shown by filled and open circles respectively, while the 3CR galaxies are shown by open triangles, except for the clear FR I radio galaxies. The FR I sources are marked with an asterisk.

range. It is also relevant to note here that de Ruiter et al. (1990) reported a strong trend for decreasing internal energy density with size, even after taking into account the correlation of size and radio power in their sample. The energy density of microwave background radiation increases steeply with redshift, and it is relevant to enquire whether our trends might be the result of a higher redshift for the giant sources. The median redshift for the GRSs is about 0.15, while for the comparison sample it is about 0.26, showing that the importance of inverse-Compton losses for the giant sources is not caused by higher redshifts for these objects. However, this illustrates that inverse-Compton losses are likely to constrain severely the number of GRSs at high redshifts, because the microwave background energy density increases as $(1 + z)^4$.

The rate of energy loss by the electrons resulting from both inverse Compton and synchrotron processes, proportional to $(B_{ic}^2 + B_{eq}^2)$, is plotted against the overall linear size for the GRSs and the comparison sample in Fig. 7(c). For the smaller sources, where synchrotron losses dominate, the rate of energy loss decreases with linear size and tapers to a minimum value of about 0.10 for the GRSs, which is set by the equivalent magnetic field of the microwave background radiation. The lifetime of a relativistic electron at an observed frequency, ν_0, resulting from both synchrotron and inverse-Compton losses is given by

$$\tau = \frac{5.03 \times 10^4}{[(1+z)\nu_0]^{1/2} B_{eq}^{3/2} [1 + (B_{ic}/B_{eq})^2]} \text{ Myr},$$

where ν_0 is in MHz and the magnetic fields B_{ic} and B_{eq} are in units of 10^{-10} T. For sources of size ~ 2 Mpc, the ratio B_{ic}/B_{eq} is about 3 (cf. Fig. 7a). For the median redshift of the giant galaxies ($z \sim 0.1$), the lifetime of the radiating electron is $\sim 2 \times 10^8$ yr at 327 MHz. The time-scale for transport of energy from the nucleus is about 7×10^7 yr for a speed of $0.1c$. Thus the source is likely to be visible well after the supply of energy to the outer lobes has ceased. These sources would be more easily detectable at low radio frequencies, and systematic searches for GRSs with sizes > 3 Mpc using telescopes such as the Giant Metrewave Radio Telescope (GMRT) would help clarify the late stages of their evolution.

4 CONSTRAINTS ON ORIENTATION AND ENVIRONMENT

To examine further whether the giant radio sources might evolve to large sizes because of a powerful nuclear engine, we investigate the relative strength of the cores as an indicator of nuclear activity. Although the degree of core prominence may vary over the lifetime of the radio source, it might be possible to arrive at statistically meaningful results. However, one must also bear in mind that in the unified schemes the strength of the core is a statistical indicator of the orientation of the source axis to the line of sight. Here, the sources at small angles to the line of sight have prominent cores compared with those at large angles, because of the effects of relativistic beaming (cf. Blandford & Königl 1979). In the unified schemes, the radio galaxies and quasars are believed to be intrinsically similar objects, but appearing to be different because of their different angles of inclination to the line of sight, with the quasars being seen at small angles while the radio galaxies lie close to the plane of the sky (Scheuer 1987; Barthel 1989; Antonucci 1993; Urry & Padovani 1995). The core flux density has been estimated from images with angular resolutions of about an arcsec or so, and any possible contamination of core flux density by small-scale jets in the intermediate luminosity objects is minimal and unlikely to affect the trends reported here.

4.1 Core prominence

There have been suggestions that the giant sources have stronger

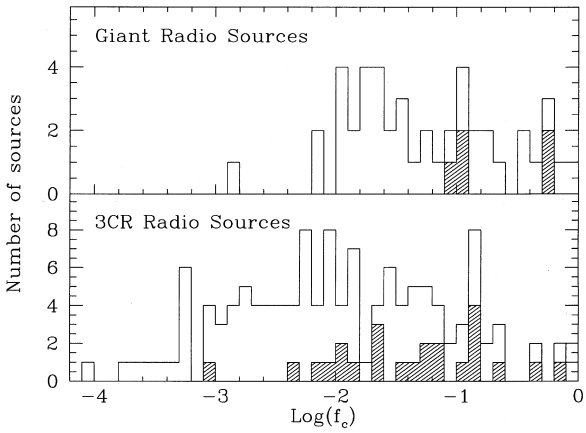

Figure 8. The distributions of f_c, the fraction of emission from the core at an emitted frequency of 8 GHz, for the samples of giant sources (upper panel) and the sample of 3CR sources with 50 kpc $< D <$ 1 Mpc (lower panel). The quasars are shown hatched in both panels.

nuclear activity, represented by more prominent cores than the smaller sources (e.g. Gopal-Krishna et al. 1989). In this section, we investigate this aspect using our sample of giant and smaller 3CR sources. In Fig. 8 we show the distributions of the fraction of emission from the core at an emitted frequency of 8 GHz, f_c, for all the giant sources (upper panel) and the complete sample of 3CR sources with sizes between 50 kpc and 1 Mpc (lower panel). The quasars are shown hatched. For both the giant sources, as well as the 3CR sources, it is clear that the quasars have more prominent cores than the radio galaxies, suggesting that the giants associated with quasars are also at smaller angles to the line of sight than the giant radio galaxies, consistent with the unified scheme. The median values of f_c for the giant quasars and radio galaxies are 0.12 and 0.034 respectively. However, for the 3CR sources in the size range 50 kpc to 1 Mpc, the median values of f_c are 0.052 and 0.0071 for the quasars and radio galaxies respectively. At first glance it appears that the giant galaxies do have more prominent cores than the smaller 3CR galaxies, and one might be tempted to suggest that they have stronger nuclear engines. The difference for the quasars needs to be examined further, because there are only five giant quasars. As many of the giant galaxies are on the borderline of the FR I/FR II classification, we examine the dependence of f_c on the total radio luminosity for the complete sample of 3CR radio sources with sizes between 50 kpc and 1 Mpc, and our sample of giant sources (Fig. 9a). There is a clear tendency of the weaker radio sources to have more prominent cores. While the fading of lobes in the giant radio sources may be a contributing factor, this is possibly caused by greater dissipation of energy close to the nucleus in the sources with low-powered radio jets. This can also be seen in the plot of the total radio luminosity against the core radio luminosity (Fig. 9b). A linear least-squares fit shows that they are related as $\log P_c = (0.44 \pm 0.043) \log P_t + (12.35 \pm 1.16)$ for galaxies and $\log P_c = (0.59 \pm 0.047) \log P_t + (8.58 \pm 1.25)$ when quasars are also included. The sample includes core flux density measurements for almost our entire sample of 3CR as well as giant radio sources. The trend is consistent with the results reported earlier by Feretti et al. (1984) and Giovannini et al. (1988), although in their studies many of the cores had reasonably high upper limits to the core flux density. A similar trend considering 3CR and B2 sources has been found by de Ruiter et al. (1990).

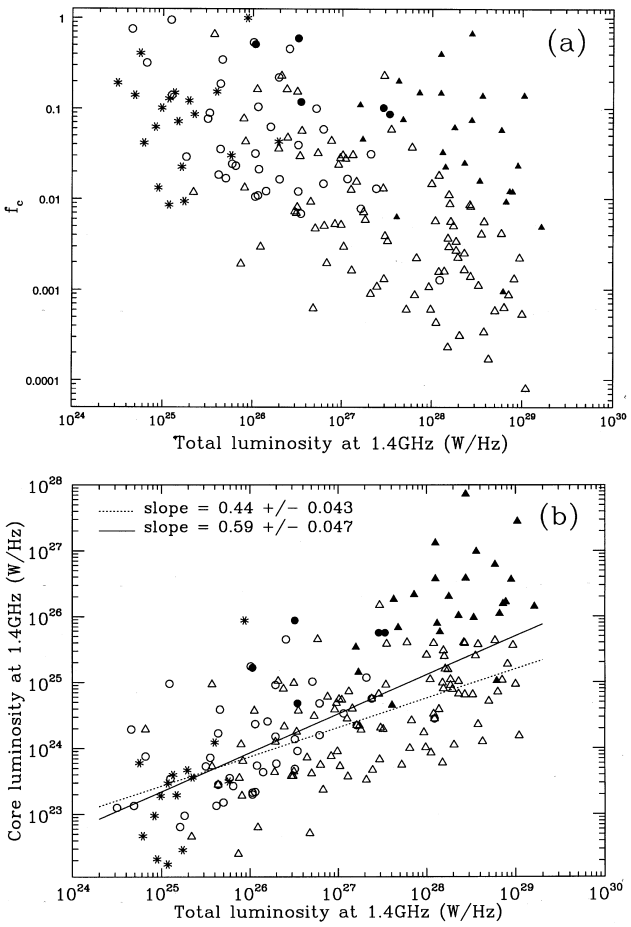

Figure 9. (a) The fraction of emission from the core and (b) the core radio luminosity plotted against the total radio luminosity of the source. The continuous line $\log P_c = (0.59 \pm 0.047) \log P_t + (8.58 \pm 1.25)$ is the linear least-squares fit including both galaxies and quasars, while the dotted line represented by $\log P_c = (0.44 \pm 0.043) \log P_t + (12.35 \pm 1.16)$ is the linear least-squares fit for galaxies only. The giant quasars and galaxies are shown by filled and open circles respectively, while the 3CR quasars and galaxies are shown by filled and open triangles respectively, except for the sources with clear FR I structure. The FR I sources have been marked with an asterisk.

Considering the giant and smaller sources of similar radio luminosity, we do not find a significant trend for the giant radio sources to have more prominent radio cores than the smaller ones. For example, in the luminosity range 10^{25} to 10^{27} W Hz^{-1}, where there is maximum overlap of the giants and the smaller sources, the median value of f_c for the giant galaxies is 0.035, compared with 0.031 for the smaller sources. This also suggests that the giants are similar objects to the normal radio sources, except for being larger and perhaps older. It is perhaps worth noting that in a couple of giant sources, such as 3C236, which has a steep-spectrum core, and 1144+352, which has a Gigahertz Peaked Spectrum (GPS) core, the high f_c values may be different from those of conventional flat-spectrum cores.

4.2 Core variability

The clear tendency for the quasar cores to be more prominent than those in galaxies, even for the giant sources, suggests that the giant quasars are also at small angles to the line of sight, consistent with

the ideas of the unified scheme. The detection of a one-sided radio jet in the giant quasar 4C74.26 (Riley & Warner 1990), and superluminal motion in the quasar 4C34.47 (Barthel et al. 1989; Hooimeyer et al. 1992) also support the unified scheme. The inferred angle to the line of sight for 4C34.47 from the observed superluminal motion is 22–44° (Barthel et al. 1989), implying that the intrinsic size is between 1.5 and 2.7 Mpc. In the quasar 4C74.26, the inferred orientation angle of $\lesssim 49°$ (Pearson et al. 1992) implies an intrinsic size $\gtrsim 2$ Mpc.

Variability of the core flux density could provide an additional test of this scenario (Blandford & Königl 1979; Saikia, Singal & Wiita 1991). We have compiled the core flux density of all the giant sources, where the epochs of measurement are also listed, but find that only four of them have core flux density measurements at more than one epoch with similar, as well as high, angular resolution. Three of these, NGC 315, NGC 6251 and 4C74.26, have been observed with the VLA with resolutions of about an arcsec, while for 4C34.47 the core flux density values are from very long baseline interferometry (VLBI) observations with mas resolution. The values for these four sources are listed in Table 4 and plotted against epoch in Fig. 10. These are at 5 GHz unless indicated otherwise in the table. For the observations made by Saikia et al. (in preparation), Bridle et al. (1979), Venturi et al. (1993) and Cotton et al. (1999), we have assumed an error of 3 per cent in the core flux density. Both the quasars 4C74.26 and 4C34.47 exhibit evidence of variability of the core flux density, with 4C34.47 varying by about 50 per cent over a 4-yr time-scale, while 4C74.26 varies by a similar amount over a 2-yr time-scale. Jägers et al. (1982) also found the core of 4C34.47 to be variable from Westerbork Synthesis Radio Telescope (WSRT) observations at 5 GHz. Both these quasars have prominent cores with f_c of

Table 4. Core flux densities.

Source name	Epoch	Flux density (mJy)	References
NGC 315	1978.56	620 ± 19	Bridle et al. (1979)
	1980.80	555 ± 20	Rudnick et al. (1986)
	1980.88	590 ± 30	Perley (1982)
	1982.55	565 ± 17	Saikia et al. in prep
	1989.29	588 ± 18	Venturi et al. (1993)
	1995.83	735 ± 22	Cotton et al. (1999)
	1996.36	695 ± 21	Cotton et al. (1999)
	1996.77	686 ± 21	Cotton et al. (1999)
	1996.84	668 ± 20	Cotton et al. (1999)
	1997.53	689 ± 21	Cotton et al. (1999)
	1990.92	#588 ± 18	Venturi et al. (1993)
	1994.53	#746 ± 22	Cotton et al. (1999)
NGC 6251	1980.88	650 ± 30	Perley (1982)
	1982.55	664 ± 20	Saikia et al. in prep
4C74.26	1986.5	420 ± 10	Riley et al. (1989)
	1987.5	370 ± 10	Riley et al. (1989)
	1988.0	310 ± 10	Riley et al. (1989)
	1988.9	328 ± 6	Pearson et al. (1992)
4C34.47	1982.27	90 ± 10	Barthel et al. (1989)
	1983.27	90 ± 5	Barthel et al. (1989)
	1986.44	110 ± 5	Barthel et al. (1989)
	1986.17	*115 ± 6	Hooimeyer et al. (1992)
	1986.40	*109 ± 5	Hooimeyer et al. (1992)
	1988.73	*141 ± 3	Hooimeyer et al. (1992)

Notes. * 10-GHz measurements; # 8-GHz measurements; other values are at 5 GHz.

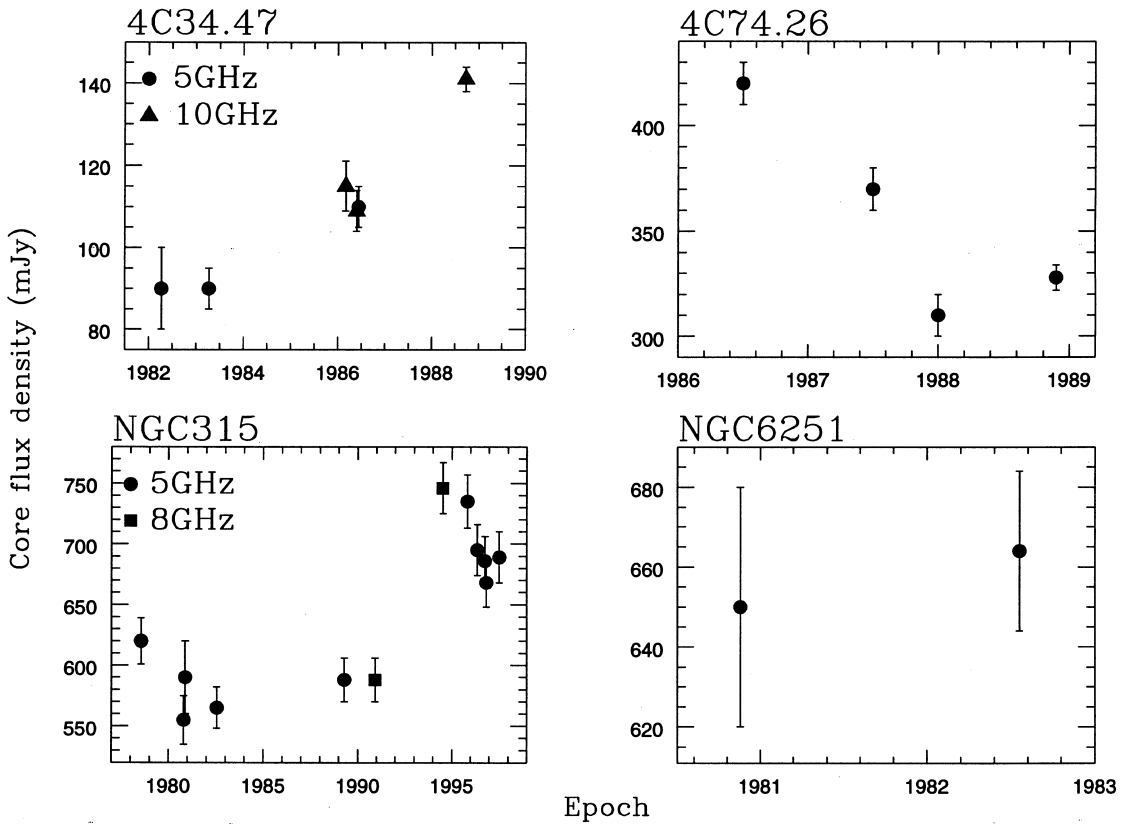

Figure 10. The flux density of the core at different epochs for the quasars (a) 4C34.47 and (b) 4C74.26, and the galaxies (c) NGC 315 and (d) NGC 6251.

about 0.60 and 0.51, respectively. Variability information is available for two of the galaxies, namely NGC 315 and NGC 6251, both of which have prominent cores with f_c of about 0.32 and 0.75 respectively. NGC 315 exhibits no evidence of significant variability over a time-scale of about 12 yr between 1978 and 1990. The core flux density of NGC 315 monitored by Ekers, Fanti & Miley (1983) also showed no evidence of variability, although their values of core flux density are slightly higher because of the poorer resolution of the observations, which would have included a part of the extended radio jet. However, Cotton et al. (1999) have reported evidence of a flare from observations around 1995 at both 5 and 8 GHz. NGC 6251 exhibits no evidence of variability over a time-scale of about 2 yr. Although the present data are rather limited, this could potentially be an important test and at present provides marginal evidence in favour of the unified scheme.

4.3 Misalignment angle

A beam of plasma advancing outwards at the same position angle will travel farther in a given time-scale compared with one for which position angle changes with time. If the formation of the giant sources is the result of such a steady ejection axis, one might find a statistical difference in the degree of misalignment between the giants and the smaller sources. However, the misalignment angle, defined to be the supplement of the angle formed at the core by the outer hotspots, shows no significant difference between the giants and the smaller sources (Fig. 11), the median values being 5 and 6° respectively for the radio galaxies, excluding those with a clear FR I structure. The median value of Δ for our Molonglo sample (IC98) is again about 5°. The values are similar when we confine ourselves to objects of similar luminosity in the range 10^{25} to $10^{27}\,\mathrm{W\,Hz^{-1}}$. The 3CR quasars exhibit a flatter distribution, which is possibly caused by projection effects in sources inclined at smaller angles to the line of sight. The distributions of the misalignment angle also suggest that the giant sources are basically similar to the smaller ones, except for being larger and perhaps older. The hotspot advance speed could depend on more rapid changes in jet direction than would be revealed by the overall misalignment angle. This might be reflected in the detailed structure of the hotspots, including multiple hotspots. However, to study this aspect reliably one needs high-resolution observations with a similar number of resolution elements along the source axes for both the giant and the smaller sources.

4.4 Separation ratio

Although, traditionally, the ratio of the separations of the hotspots from the nucleus for a randomly oriented sample of sources has been used to estimate the hotspot advancement speed (cf. Longair & Riley 1979), it has become clear over the years that an asymmetric environment is also responsible for the observed separation ratios (Saikia 1981; McCarthy, van Breugel & Kapahi 1991; Scheuer 1995). There has been some evidence that the compact steep-spectrum sources, which are of subgalactic dimensions, have larger separation ratios, suggesting that they are evolving in an asymmetric environment (Saikia et al. 1995). As the sources advance outwards into a more symmetric environment on opposite sides and with the jets maintaining a constant opening angle, the sources tend to become more symmetric (Saikia et al. 1996). The sample of 3CR sources considered by Saikia et al. showed some evidence in support of such a scenario.

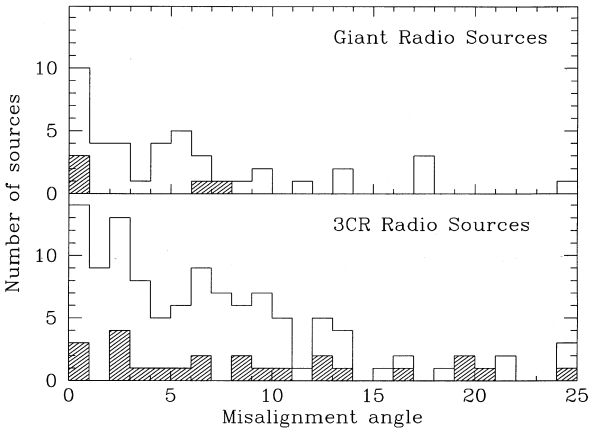

Figure 11. The distributions of the misalignment angle, Δ, defined to be the supplement of the angle formed at the core by the outer hotspots in degrees, for the samples of giant sources (upper panel) and the sample of 3CR sources with $50\,\mathrm{kpc} < D < 1\,\mathrm{Mpc}$ (lower panel). The quasars are shown hatched in both panels.

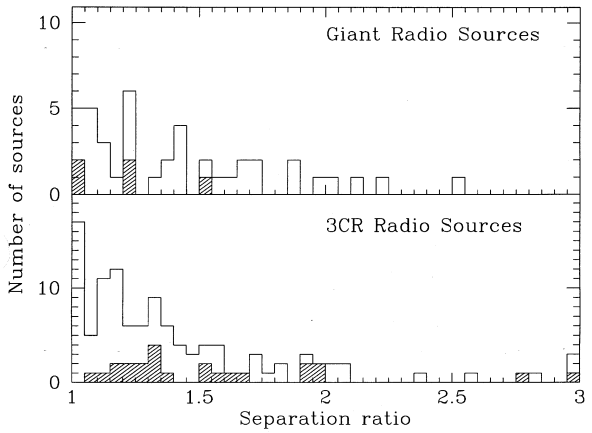

Figure 12. The distributions of the separation ratio, r_θ, defined to be the ratio of the separation of the farther hotspot or peak of emission from the nucleus to that of the nearer one on the opposite side, for the samples of giant sources (upper panel) and the sample of 3CR sources with $50\,\mathrm{kpc} < D < 1\,\mathrm{Mpc}$ (lower panel). The quasars are shown hatched in both panels.

Here we attempt to probe the environment on Mpc scales by examining the separation ratio of the giant radio sources (Fig. 12). Considering all the sources in the luminosity range 10^{25} to $10^{27}\,\mathrm{W\,Hz^{-1}}$, so that the objects are of similar luminosity, the median value of the Giant Radio Galaxies (GRGs) is about 1.39, which is marginally higher than for the smaller sized 3CR radio galaxies with projected sizes between 50 kpc and 1 Mpc, which has a median value of 1.19. The corresponding values for the entire sample are 1.36 and 1.23 respectively. The median value for our Molonglo sample (IC98) is 1.26, which is similar to that for the 3CR sources. We have excluded all sources with a clear FR I structure. Although the difference is only marginally significant, the giant sources do not appear to be more symmetric and their observed asymmetry could be caused by either the beams encountering density gradients on the scale of Mpc associated with groups and clusters of galaxies after they travel out of the halo of the parent galaxy, or the jets travelling outwards with constant jet widths after they emerge from an asymmetric

environment. The jet widths could remain constant if they were confined by toroidal magnetic fields (Appl 1996; Appl & Camenzind 1993a,b). One can probe the asymmetry in the environment by examining the relationship between jet-sidedness and the separation ratio. There are only four galaxies, namely NGC 315, 0319 − 454, 4C74.17 and NGC 6251, and two quasars, 4C74.26 and 4C34.47, with well-defined radio jets satisfying the criteria suggested by Bridle & Perley (1984). The jet side is closer in three of the four galaxies, but farther in both the quasars, consistent with the environment playing a stronger role for galaxies while in quasars the effects of orientation seem more significant. The basic trends expected in the unified scheme are also seen in the giant radio sources. The flatter distribution of r_θ for the 3CR quasars is possibly caused by their smaller angles of inclination to the line of sight.

5 CONCLUDING REMARKS

We have presented VLA observations of the giant quasars 0437−244 and 1025−229 from the Molonglo Complete Sample. These sources have well-defined FR II radio structure, possible one-sided jets, no significant depolarization between 1365 and 4935 MHz and low rotation measure ($|\mathrm{RM}| < 20\,\mathrm{rad\,m^{-2}}$). We have compiled a sample of 53 known giant radio sources from the literature, and have compared some of their properties with those of a complete sample of 3CR radio sources with sizes between 50 kpc and 1 Mpc to investigate the evolution of giant sources, and test their consistency with the unified scheme for radio galaxies and quasars. The conclusions are summarized briefly here.

(i) The power–linear size or P–D diagram for the 3CR and giant sources shows a deficit of sources with radio luminosity greater than about $2 \times 10^{27}\,\mathrm{W\,Hz^{-1}}$ at 1.4 GHz and sizes larger than 1 Mpc. A similar trend was noted earlier by Kaiser et al. (1997), and appears to be true for this much larger sample of giant sources selected from samples covering a wide flux density range. The location of the giants in the P–D diagram suggests that they have evolved from the smaller sources. Suggestions that they might be of similar age to the smaller sources from spectral index studies should be treated with caution, because of the large number of uncertainties and assumptions in these estimates.

(ii) The equipartition magnetic field, B_{eq}, is smaller than the equivalent magnetic field of the microwave background radiation, B_{ic}, for the giant sources, while the reverse is true for the smaller sources. Thus inverse-Compton losses dominate for the giant radio sources, while synchrotron radiation losses are more important for the smaller sources. This is likely to limit the number of giant radio sources severely at large redshifts.

(iii) We find an inverse correlation between the degree of core prominence and total radio luminosity, and show that the giant radio sources have similar core strengths to the smaller sources when sources of similar total luminosity are considered. Although many of the giants have stronger cores than the high-luminosity FR II radio sources (cf. Saikia & Kulkarni 1994), this is largely because of the inverse correlation between the degree of core prominence and total radio luminosity, and does not necessarily indicate higher nuclear activity or a more powerful central engine. The more prominent cores in the lower luminosity sources are possibly caused by greater dissipation of energy by the radio jet close to the nucleus.

(iv) The degree of collinearity for the giant radio sources is similar to that of the smaller sources, suggesting that the steadiness of the axis is not the determining factor for the formation of giant radio sources.

(v) The ratio of separation of the outer hotspots for the giant sources appears marginally larger than for the smaller sized sources. This is somewhat surprising and could possibly be caused by interaction of the energy-carrying beams with cluster-sized density gradients far from the parent galaxy. Out of six sources with radio jets, the hotspot on the jet side is closer for three of the four galaxies, but neither of the two quasars. This suggests that the environment plays a stronger role for galaxies, while in quasars the effects of orientation seem more significant.

(vi) The giant quasars have more prominent cores, one of which, 4C34.47, exhibits superluminal motion, and the cores of both quasars with adequate data exhibit evidence of variability. Unlike the quasars, the radio cores of one of the galaxies, NGC 6251, exhibits no evidence of significant variability, while the other, NGC 315, exhibits evidence of a flare around 1995 after maintaining a nearly constant flux density for about 20 yr including the observations of Ekers et al. (1981). Although the available data are very limited, these are consistent with the unified schemes for radio galaxies and quasars.

ACKNOWLEDGMENTS

We thank Sivakumar Manickam and Divya Oberoi for computational help, an anonymous referee for meticulously reading the manuscript and making several helpful suggestions and comments, Jayaram Chengalur and Kandaswamy Subramanian for their comments on the manuscript and many of our colleagues for useful discussions. The National Radio Astronomy Observatory is a facility of the National Science Foundation operated under cooperative agreement by Associated Universities Inc. We thank the staff of the Very Large Array for the observations. This research has made use of the NASA/IPAC extragalactic database (NED) which is operated by the Jet Propulsion Laboratory, Caltech, under contract with the National Aeronautics and Space Administration.

REFERENCES

Alexander P., Leahy J. P., 1987, MNRAS, 225, 1
Antonucci R., 1993, ARA&A, 31, 473
Appl, S., 1996, in Hardee P. E., Bridle A. H., Zensus J. A. eds, ASP Conf. Ser. Vol. 100, Energy Transport in Radio Galaxies and Quasars. Astron. Soc. Pac., San Francisco, p. 129
Appl S., Camenzind M., 1993a, A&A, 270, 71
Appl S., Camenzind M., 1993b, A&A, 274, 699
Baldwin, J. E., 1982, in Heeschen D. S., Wade C. M., eds, Proc. IAU Symp. 97, Extragalactic Radio Sources. Reidel, Dordrecht, p. 21
Barthel P. D., 1987, in Zensus J. A., Pearson T. J., eds, Superluminal Radio Sources. Cambridge Univ. Press, Cambridge, p. 148
Barthel P. D., 1989, ApJ, 336, 606
Barthel P. D., Schilizzi R. T., Miley G. K., Jägers W. J., Strom R. G., 1985, A&A, 148, 243
Barthel P. D., Hooimeyer J. R., Schilizzi R. T., Miley G. K., Preuss E., 1989, ApJ, 336, 601
Bhatnagar S., Gopal-Krishna, Wisotzki L., 1998, MNRAS, 299, L25
Blandford R. D., Königl A., 1979, ApJ, 232, 34
Blundell K. M., Rawlings S., Willott C. J., 1999, AJ, 117, 677
Bridle A. H., Perley R. A., 1984, ARA&A, 22, 319
Bridle A. H., Davis M. M., Meloy D. A., Fomalont E. B., Strom R. G., Willis A. G., 1976, Nat, 262, 179

Bridle A. H., Davis M. M., Fomalont E. B., Willis A. G., Strom R. G., 1979, ApJ, 228, L9
Cotter G., Rawlings S., Saunders R., 1996, MNRAS, 281, 1081
Cotton W. D., Feretti L., Giovannini G., Lara L., Venturi T., 1999, ApJ, 519, 108
Danziger, I. J., Goss, W. M., Frater, R. H., 1978, MNRAS, 184, 341
de Bruyn A. G., 1989, A&A, 226, L13
de Bruyn A. G., Schoenmakers A. P., Röttgering H., van der Laan H., 1998, NFRA Newsl., 15, 21
de Ruiter H. R., Parma P., Fanti C., Fanti R., 1990, A&A, 227, 351
Eilek J. A., Melrose D. B., Walker M. A., 1997, ApJ, 483, 282
Ekers R. D., Fanti R., Lari C., Parma P., 1981, A&A, 101, 194
Ekers R. D., Fanti R., Miley G. K., 1983, A&A, 120, 297
Fanaroff B. L., Riley J. M., 1974, MNRAS, 167, L31
Feretti L., Giovannini G., Gregorini L., Parma P., Zamorani G., 1984, A&A, 139, 55
Fernini I., Burns J. O., Bridle A. H., Perley R. A., 1993, AJ, 105, 1690
Fernini I., Burns J. O., Perley R. A., 1997, AJ, 114, 2292
Giovannini G., Feretti L., Gregorini L., Parma P., 1988, A&A, 199, 73
Gopal-Krishna , Wiita P. J., Saripalli L., 1989, MNRAS, 239, 173
Gregorini L., Padrielli L., Parma P., Gilmore G., 1988, A&AS, 74, 107
Hardcastle M. J., Alexander P., Pooley G. G., Riley J. M., 1997, MNRAS, 288, 859
Hine R. G., 1979, MNRAS, 189, 527
Hooimeyer J. R. A., Barthel P. D., Schilizzi R. T., Miley G. K., 1992, A&A, 261, 1
Ishwara-Chandra C. H., Saikia D. J., Kapahi V. K., McCarthy P. J., 1998, MNRAS, 300, 269 (IC98)
Jägers, W.J., 1986, PhD thesis, Univ. Leiden
Jägers W. J., van Breugel W. J. M., Miley G. K., Schilizzi R. T., Conway R. G., 1982, A&A, 105, 278
Johnson R. A., Leahy J. P., Garrington S. T., 1995, MNRAS, 273, 877
Jones P. A., McAdam W. B., 1992, ApJS, 80, 137
Kaiser C. R., Alexander P., 1997, MNRAS, 286, 215
Kaiser C. R., Dennett-Thorpe J., Alexander P., 1997, MNRAS, 292, 723
Kapahi V. K., Athreya R. M., Subrahmanya C. R., Baker J. C., Hunstead R. W., McCarthy P. J., van Breugel W., 1998a, ApJS, 118, 327
Kapahi V. K., Athreya R. M., van Breugel W., McCarthy P. J., Subrahmanya C. R., 1998b, ApJS, 118, 275
Kronberg P. P., Wielebinski R., Graham D. A., 1986, A&A, 169, 63
Lacy M., Rawlings S., Saunders R., Warner P. J., 1993, MNRAS, 264, 721
Laing R., Riley J. M., Longair M., 1983, MNRAS, 204, 151
Large M. I., Mills B. Y., Little A. G., Crawford D. F., Sutton J. M., 1981, MNRAS, 194, 693
Leahy J. P., Perley R. A., 1991, AJ, 102, 537
Leahy J. P., Williams A. G., 1984, MNRAS, 210, 929
Leahy J. P., Muxlow T. W. B., Stephens P. W., 1989, MNRAS, 239, 401
Longair M. S., 1994, High Energy Astrophysics, Cambridge Univ. Press, Cambridge
Longair M. S., Riley J. M., 1979, MNRAS, 188, 625
McCarthy P. J., van Breugel W., Kapahi V. K., 1991, ApJ, 371, 478
Machalski J., Condon J. J., 1985, AJ, 90, 5
Mack K. H., Klein U., O'Dea C. P., Willis A. G., Saripalli L., 1998, A&A, 329, 431
Masson C. R., 1979, MNRAS, 187, 253
Miley G. K., 1980, ARA&A, 18, 165
Myers S. T., Spangler S. R., 1985, ApJ, 291, 52
Neeser M. J., Eales S. A., Law-Green J. D., Leahy J. P., Rawlings S., 1995, ApJ, 451, 76
Pacholczyk A. G., 1977, Radio Galaxies, Pergamon Press, Oxford
Parma P., de Ruiter H. R., Mack K. H., van Breugel W., Dey A., Fanti R., Klein U., 1996, A&A, 311, 49
Pearson T. J., Blundell K. M., Riley J. M., Warner P. J., 1992, MNRAS, 259, L13
Perley R. A., 1982, AJ, 87, 859
Rengelink R., Tang Y., de Bruyn A. G., Miley G. K., Bremer M. N., Röttgering H. J. A., Bremer M. A. R., 1997, A&AS, 124, 259
Riley J. M., Warner P. J., 1990, MNRAS, 246, L1
Riley J. M., Warner P. J., Rawlings S., Saunders R., Pooley G. G., Eales S. A., 1989, MNRAS, 236, L13
Röttgering H. J. A., Tang T., Bremer M. A. R., de Bruyn A. G., Miley G. K., Rengelink R. B., Bremer M. N., 1996, MNRAS, 282, 1033
Rudnick L., Jones T. W., Fiedler R., 1986, AJ, 91, 1011
Saikia D. J., 1981, MNRAS, 197, L11
Saikia D. J., Kulkarni V. K., 1994, MNRAS, 270, 897
Saikia D. J., Singal A. K., Wiita P. J., 1991, in Miller H. R., Wiita P. J., eds, Variability of Active Galactic Nuclei. Cambridge Univ. Press, Cambridge, p. 160
Saikia D. J., Jeyakumar S., Wiita P. J., Sanghera H. S., Spencer R. E., 1995, MNRAS, 276, 1215
Saikia, D. J., Jeyakumar, S., Wiita, P. J., Hooda, J. S., 1996, in Fanti C., Fanti R., O'Dea C. P., Schilizzi R. T., eds, Proc. Dwingeloo Workshop on Compact Steep Spectrum and GHz Peaked Spectrum Radio Sources. Istituto di Radioastronomia, Bologna, p. 252
Saripalli, L., 1988, PhD thesis, Indian Inst. Science, Bangalore
Saripalli L., Gopal-Krishna , Reich W., Kühr H., 1986, A&A, 170, 20
Saripalli L., Subrahmanyan R., Hunstead R. W., 1994, MNRAS, 269, 37
Saripalli L., Mack K. H., Klein U., Strom R., Singal A. K., 1996, A&A, 306, 708
Saunders R., Baldwin J. E., Warner P. J., 1987, MNRAS, 225, 713
Scheuer P. A. G., 1974, MNRAS, 166, 513
Scheuer P. A. G., 1987, in Zensus J. A., Pearson T. J., eds, Superluminal Radio Sources. Cambridge Univ. Press, Cambridge, p. 104
Scheuer P. A. G., 1995, MNRAS, 277, 331
Schoenmakers A. P., Mack K. H., Lara L., Röttgering H. J. A., de Bruyn A. G., van der Laan H., Giovannini G., 1998, A&A, 336, 455
Schoenmakers A. P., de Bruyn A. G., Röttgering H. J. A., van der Laan H., 1999, A&A, 341, 44
Shklovskii I., 1963, SvA, 6, 465
Strom R. G., Willis A. G., 1980, A&A, 85, 36
Strom R. G., Baker J. R., Willis A. G., 1981, A&A, 100, 220
Subrahmanya C. R., Hunstead R. W., 1986, A&A, 170, 27
Subrahmanyan R., Saripalli L., 1993, MNRAS, 260, 908
Subrahmanyan R., Saripalli L., Hunstead R. W., 1996, MNRAS, 279, 257
Urry C. M., Padovani P., 1995, PASP, 107, 803
van Breugel W. J. M., Willis A. G., 1981, A&A, 96, 332
Venturi T., Giovannini G., Feretti L., Comoretto G., Wehrle A. E., 1993, ApJ, 408, 81
Vigotti M., Grueff G., Perley R. A., Clark B. G., Bridle A. H., 1989, AJ, 98, 419
Waggett P. C., Warner P. J., Baldwin J. E., 1977, MNRAS, 181, 465
Willis A. G., Strom R. G., 1978, A&A, 62, 375
Willis A. G., Strom R. G., Wilson A. S., 1974, Nat, 250, 625
Willis A. G., Strom R. G., Bridle A. H., Fomalont E. B., 1981, A&A, 95, 250
Willis, A. G., Strom, R. G., Perley, R. A., Bridle, A. H., 1982, in Heeschen D. S., Wade C. M., eds, IAU Symp. 97, Extragalactic Radio Sources. Reidel, Dordrecht, p. 141

This paper has been typeset from a TEX/LATEX file prepared by the author.